DEBONDING DETECTION IN CFRP BONDED STRUCTURES USING PROPAGATION PROPERTIES OF LAMB WAVES

Yoji Okabe*, Kazuki Natori*, Nobuo Takeda*, Toshimichi Ogisu**
*Dept. of Aeronautics and Astronautics, School of Engineering, Univ. of Tokyo
7-3-1 Hongo, Bunkyo-ku, Tokyo 113-8656, JAPAN
, **Fuji Heavy Industries Ltd., Aerospace Company

Abstract

Carbon fiber reinforced plastic (CFRP) laminates are being used for the primary structures in the latest airplanes. However, bonded composite structures have a possibility of introducing debonding. Thus, the authors have constructed a debonding detection system using Lamb waves and attempted to apply the system to CFRP skin/stringer structures. In this research, in order to evaluate the debonding length without reference database, we used two sensors: one on the surface of the stringer and the other on the surface of the skin. When a debonding appeared in the adhesive layer, the received waves became different between the two sensors because of changes in the propagation length and the energy density. Hence, this system succeeded in evaluating the debonding length quantitatively from the arrival time difference and the amplitude ratio between the two sensors.

1 Introduction

CFRP laminates have increasingly become popular materials and are applied to primary structures in the latest civil aircrafts. For jointing of the CFRP laminates, adhesion is more suitable than mechanical joints with bolts or rivets. However, bonded composite structures have a possibility of introducing debonding in the bonding line, which is a critical damage to the structures. Current non-destructive inspection methods are not efficient to detect debonding in the inaccessible areas and result in extensive time and costs. For monitoring the condition of the CFRP structures, structural health monitoring systems using ultrasonic waves generated and received by pre-installed actuators

and sensors are promising and cost-effective means [1-2]. As one of the systems, the authors are constructing a debonding detection system using Lamb waves, which are generated by a piezo-ceramic (PZT) actuator and received by a fiber Bragg grating (FBG) sensor, and attempting to apply the system to CFRP skin/stringer structures [3].

In our previous research, one sensor was bonded on the surface of the stringer or embedded in the adhesion layer between the skin and the stringer [4]. Then, ultrasonic wave was generated by a PZT on the skin and propagated through the debonded region. After that the wavelet transform was applied to the waves received by the sensor, and the mean-square damage index and the correlation coefficient were calculated from the wavelet coefficients. As a result, the debonding length could be evaluated using these indexes. However, this method needs reference database because the rates of the change in the indexes have individual differences. In order to solve this problem, we use two sensors in this research: one on the upper surface of the stringer and the other on the lower surface of the skin, and attempt to evaluate the debonding length quantitatively from the difference of the arrival time and the ratio of the maximum amplitude between the two sensors. This diagnosis method does not require reference database, and the information extracted from the waveforms are really simple.

2 Principle of debonding evaluation

The skin/stringer structure that the authors assume to apply our debonding detection system to is shown in Fig. 1. The stringer is hat shape, and the debonding between the skin and the stringer appears from the end of the stringer. In order to detect the debonding, ultrasonic waves are

propagated through the debonded region. One piezo-ceramic (PZT) actuator and two fiber Bragg grating (FBG) sensors, which are a kind of optical fiber sensors, are located as shown in Fig. 2. One FBG sensor is bonded on the top surface of the stringer, and the other is on the bottom surface of the skin. The waveforms received by these two sensors become different after occurrence of the debonding. Thus, comparison of the two waves is effective means to evaluate the debonding progress.
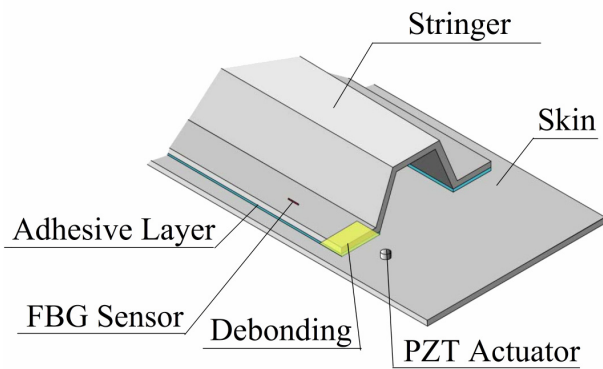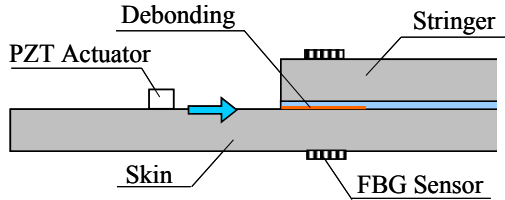

Fig. 1. Skin/stringer structure.

Fig. 2. Location of a PZT and two FBG sensors.

3 Experimental setup

In this research, simple coupon specimens simulating the skin/stringer structure were prepared. The dimensions are illustrated in Fig. 3. Two CFRP quasi-isotropic laminates (T700S/2500, TORAY, $[45/0/-45/90]_{3s}$) were bonded in the secondary bonding process using adhesive films (Metlbond 1515-3M). As a feasibility study, PZT sensors are used instead of FBG sensors. As shown in Fig. 4, one of the specimens is intact and the other has debonding. The debonding was introduced by the following procedures; artificial defect of 2mm was introduced using a Kapton film embedded during the bonding process, and the debonding was developed by insertion of a cutting blade into the artificial defect. A three-cycle sine wave of 100kHz with a hamming window as shown in Fig. 5 was used to drive the PZT actuator. A propagating ultrasonic

wave was received by PZT sensors on the upper and lower laminates of the specimens. The positions of the sensors were changed from $L = 2$mm to 30mm at 2mm intervals.
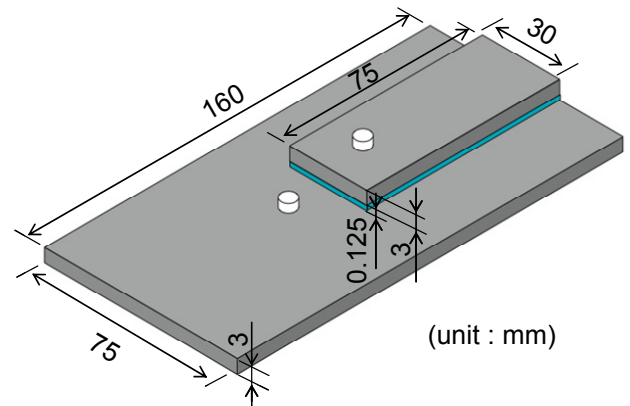

Fig. 3. Simple coupon specimen simulating the skin/stringer structure.
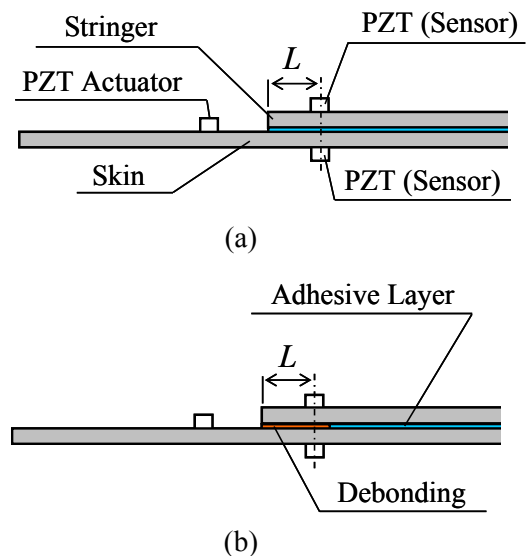

(a)

(b)

Fig. 4. Configuration of the specimens and locations of PZTs: (a) perfectly bonded and (b) with debonding.
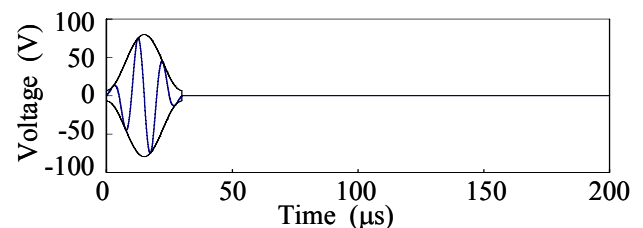

Fig. 5. Three-cycle windowed sine burst signal to drive the PZT actuator.

Fig. 6 shows the cross-section photograph of the specimen with the debonding. It is clear that the debonding length is about 16mm from the edge of the upper laminate. Soft X-ray apparatus (SOFTEX, M-100S) was also used to observe the debonding shape. As a result, the debonding length was found to be constant of 16mm over the whole width of the upper laminate.
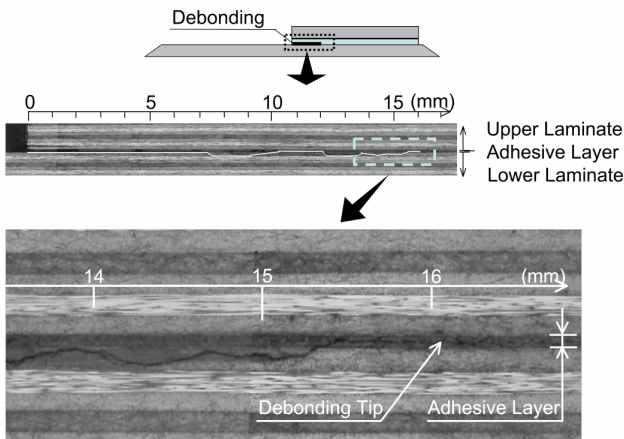

Fig. 6. Cross-section observation of the specimen with debonding.

4 Experimental results

Fig. 7 shows the output of the PZT sensors located at L = 10mm for the perfectly bonded structure, and Fig. 8 shows the outputs for the structure with debonding. The envelopes of the waves calculated using Hilbert transform [1] are also plotted in the graphs. As shown in Fig. 7(a), maximum amplitude A_m is defined as maximum value of the envelope curves, and arrival time T_a as the time when the envelope curve becomes maximum. It is clear from Fig. 7 that the waveforms measured by the PZT sensors on the upper and the lower laminates in the perfectly bonded structure are almost the same except the phase difference. In contrast, the A_m of the PZT sensor on the upper laminate in the structure with debonding is much smaller than that on the lower laminate (Fig. 8).

The A_m and T_a are plotted as a function of the sensor position from L = 2mm to 30mm in Figs. 9 and 10 respectively. As shown in Fig. 9, it is clear that the A_m on the upper laminate becomes smaller and that on the lower laminate becomes larger in the debonded region of the specimen with debonding than that of the perfectly bonded specimen. In addition, the T_a on upper laminate in the debonded region was delayed as shown in Fig. 10. These

changes are because the ultrasonic wave propagates around the debonding tip to the upper laminate since the ultrasonic wave cannot pass through the debonding. Hence the wave to the upper sensor is attenuated and delayed.
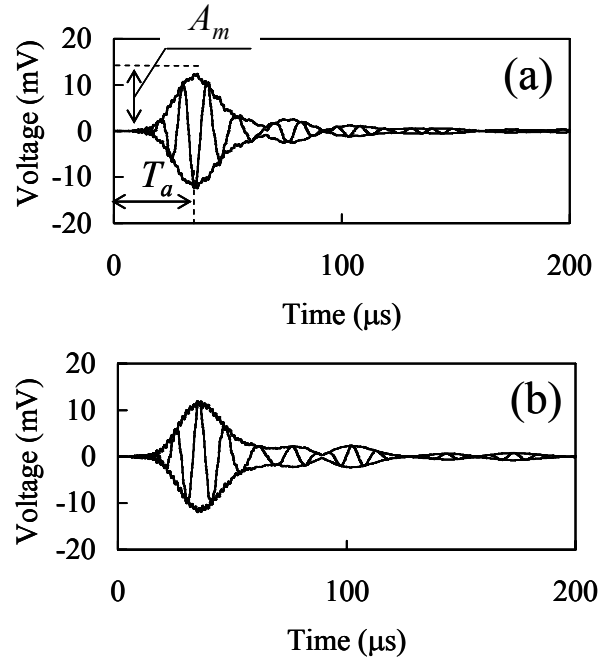

Fig. 7. Waves at L = 10mm for the bonded structure: (a) on upper laminate and (b) on lower laminate.

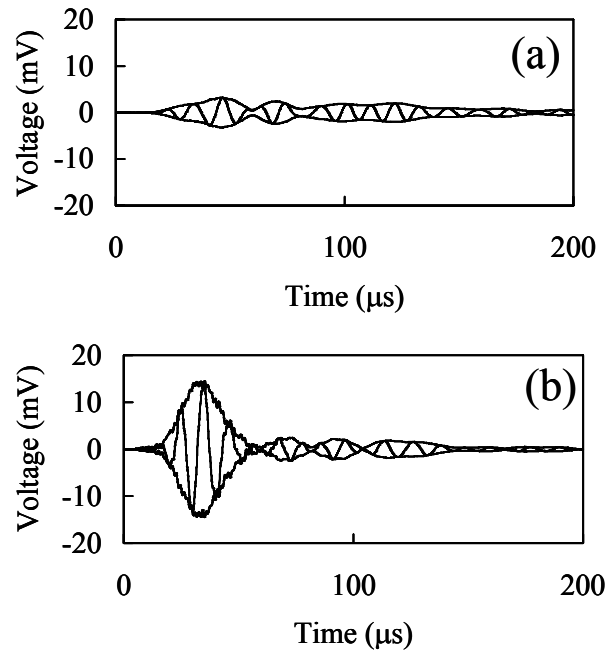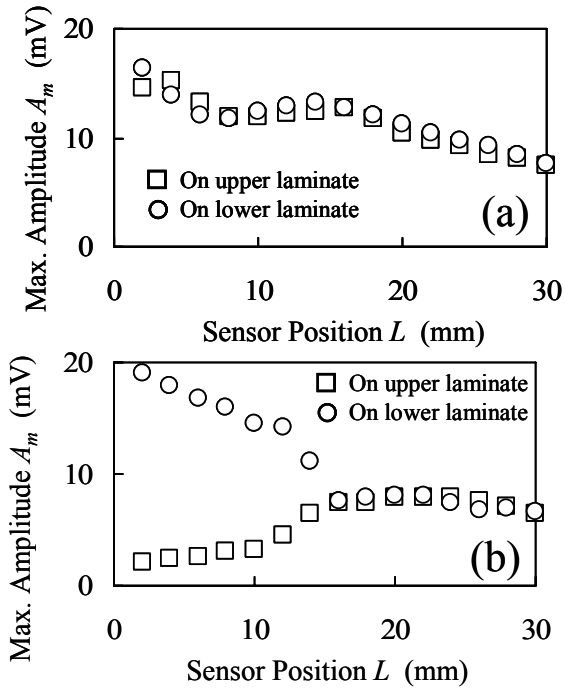Fig. 8. Waves at L = 10mm for the debonded structure: (a) upper and (b) lower.

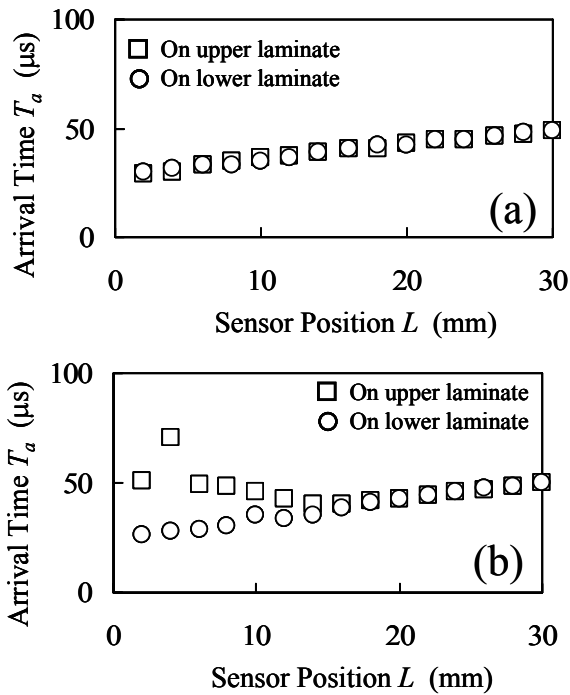Fig. 9. Maximum amplitude A_m: (a) perfectly bonded structure and (b) structure with debonding.

Fig. 10. Arrival time T_a: (a) perfectly bonded structure and (b) structure with debonding.

5 Numerical simulation

In order to confirm the phenomenon observed through the experiments, numerical simulation of the wave propagation was conducted with finite element method (FEM) using ABAQUS/Explicit.

Fig. 11 shows the finite element model simulating the simple bonded specimen used in the experiment. Since the wavelength of A_0 mode was found to be about 14mm under this condition by theoretical calculation [5], dimensions of every rectangular solid element were set to $1 \times 1 \times 1mm^3$. The ultrasonic waves were generated by application of pressure at the position shown in Fig. 11 as the three-cycle sine wave of 100kHz with a hamming window. The debonding between the skin and the adhesive layer was simulated by a slit of 25μm in thickness.
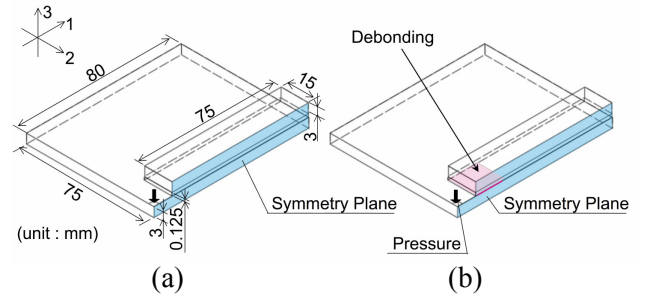

Fig. 11 Finite element models: (a) intact specimen and (b) damaged specimen.

As an example of the simulation results, the distribution of Mises stress in the symmetry plane in 30μs after the wave generation is plotted in Fig. 12. In the intact model, the Lamb wave propagates through the structure treating the skin and the stringer as one integrated plate. When the debonding exists, however, the wave propagates around the debonding tip to the stringer. Hence the arrival time to the upper sensor is delayed and the wave energy becomes different between the upper and the lower sensors.
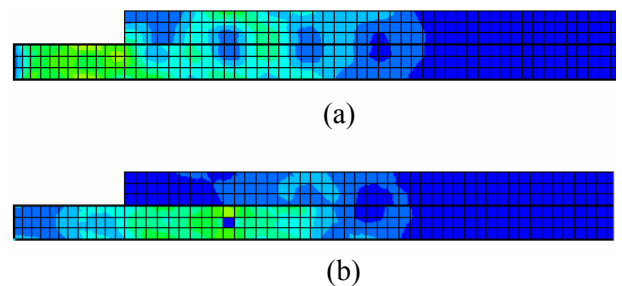

Fig. 12. Mises stress distribution at 30μs: (a) perfectly bonded structure and (b) structure with debonding.

Then the time history of acceleration in the thickness direction was extracted as sensor output at each sensor position, and the maximum amplitude and the arrival time were obtained from the acceleration time history corresponding to the experimental results in Figs. 9 and 10. The obtained results are plotted in Figs. 13 and 14. Since these calculation results well reproduced the experimental results, it was confirmed that the change in the waveforms observed in the experiments were caused by the wave propagation around the delamination tip.
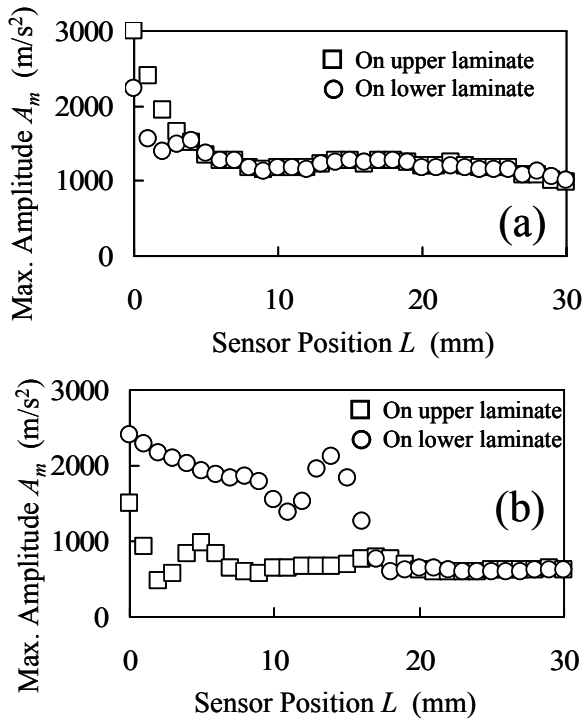

Fig. 13. Maximum amplitude A_m obtained by numerical simulation: (a) perfectly bonded structure and (b) structure with debonding.

6 Proposal of indexes for debonding detection

From the experiment and the numerical simulation, we propose two effective indexes for quantitative evaluation of the debonding progress. One of the indexes is the amplitude ratio R_m defined by the ratio of A_m of the upper sensor to that of the lower sensor, and the other is the arrival time difference ΔT_a defined by the difference of T_a between the two sensors.

Fig. 15 shows the R_m obtained by the experiment (Fig. 9) and the numerical calculation (Fig. 13). Although the R_m is almost 1 in the intact region, that in the debonded area decreases
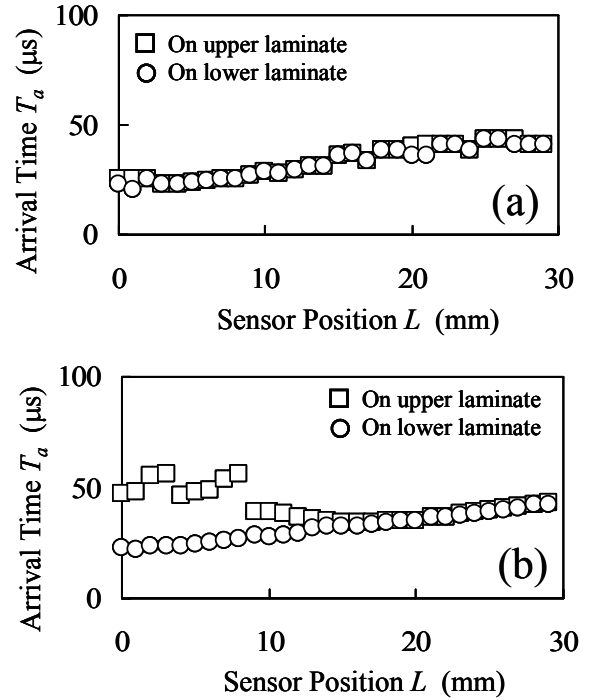

Fig. 14. Arrival time T_a obtained by numerical simulation: (a) perfectly bonded structure and (b) structure with debonding.

drastically. Then the ΔT_a obtained by the experiment (Fig. 10) and the calculation (Fig. 14) are plotted in Fig. 16. The ΔT_a increases in proportion to the distance between the debonding tip and the sensor position in the debonded area. These tendencies of the R_m and the ΔT_a are considered to be correlated with the relative position of the sensor and the debonding tip. Thus, in the actual situation, one pair of the sensors located near the stringer edge seems sufficient to evaluate the debonding progress. The occurrence of the debonding is detected by the R_m and the debonding length is estimated by the ΔT_a.

7 Conclusions

In this research, PZT sensors were set on the both surfaces of the skin/stringer bonded structure and received Lamb waves that was generated by a PZT actuator put on the skin surface. Through the experiment and the numerical simulation for the wave propagation, it was found that the comparison of the waveforms received by the two sensors was effective to detect the debonding in the bonded structures. The amplitude ratio certainly showed the presence of the debonding at the sensor position, and the arrival time difference was capable of evaluating the debonding length from the sensor point.

Consequently, the debonding progress was successfully evaluated quantitatively using these indexes. This diagnosis method does not require reference database since the waves received by the two sensors are compared, and the information extracted from the waveforms are really simple. Thus, the evaluation method of the debonding length increased simplicity and robustness.

In the future, we will apply FBG sensors instead of PZT sensors. Although PZT sensors are obstacle on the surface of the skin for practical use, FBG sensors can be embedded near the surface of the skin laminate.
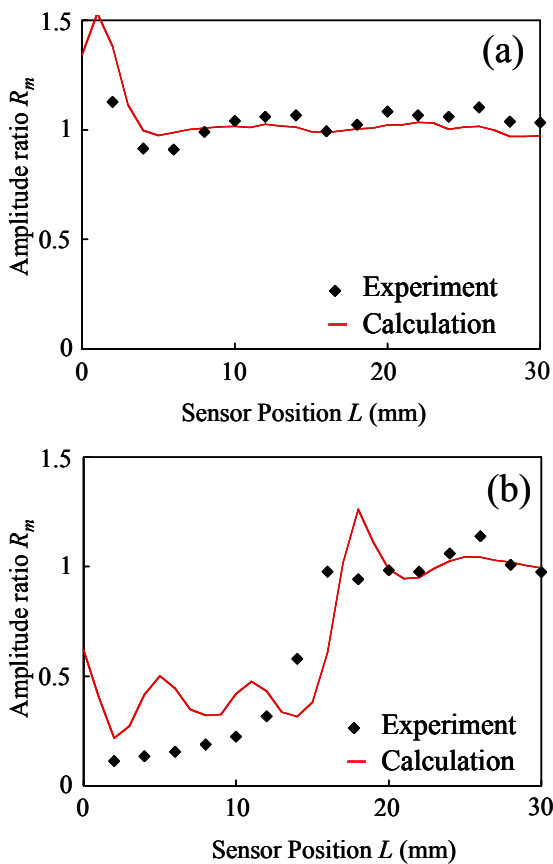
Acknowledgements

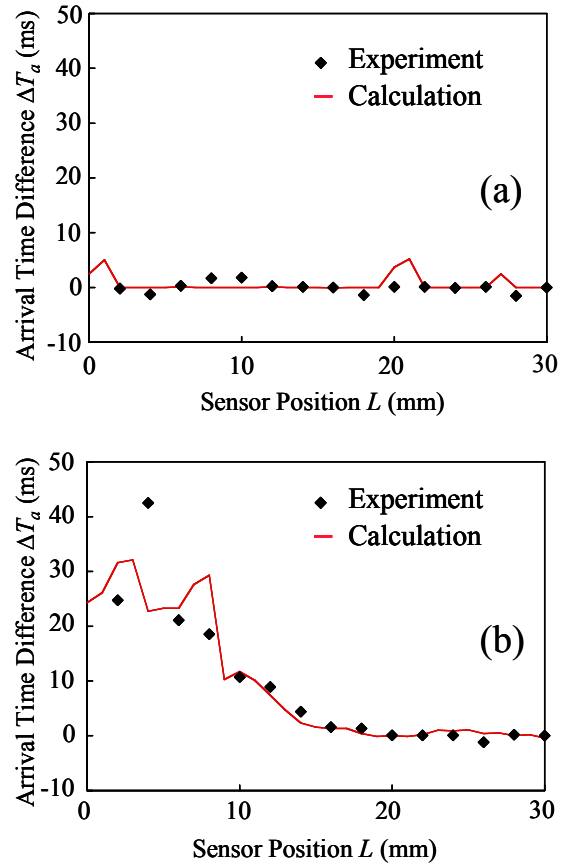Fig. 15. Amplitude ratio R_m: (a) perfectly bonded structure and (b) structure with debonding.

Fig. 16. Arrival time difference ΔT_a: (a) perfectly bonded structure and (b) structure with debonding.

References

[1] Staszewski W., Boller C. and Tomlinson G. "*Health Monitoring of Aerospace Structures*". John Willy & Sons, 2004.
[2] Kessler S.S., Spearing S.M. and Atalla M.J. "In-situ damage detection of composites structures using Lamb wave methods". *Proc. First European Workshop on Structural Health Monitoring*, Paris, pp 374-381, 2002.
[3] Ogisu T., Shimanuki M., Kiyoshima S., Okabe Y. and Takeda N. "Feasibility studies on active damage detection for CFRP aircraft bonding structures". *Adv. Compos. Mater.*, Vol.15, No. 2, pp 153-173, 2006.
[4] Okabe Y., Kuwahara J., Takeda N., Ogisu T., Kojima S. and Komatsuzaki S. "Evaluation of debonding progress in composite bonded structures by ultrasonic wave sensing with fiber Bragg grating sensors". *Proc. SPIE*, San Diego, Vol. 6179, 61790G, 2006.
[5] Nayfeh A.H. "*Wave Propagation in Layered Anisotropic Media with Applications to Composites*". Elsevier, 1995.